

Supporting Information

for

Concave Octopus-Like PtCu Nanoframes Mediated Photo-Electro Fenton Catalysis for Fast Organic Dyestuff Elimination

Yangyang Yan,^{†a} Shaowen Cheng,^{†a} Ping Zhou,^a Heying Li,^{a, b} Xiaoran Liu,^a Manping Lin,^a Feihu Xie,^b Keke Zhang,^{b*} Yi Zhang,^b Chenyang Zhang,^b Shuang Zhao,^c Jiahua Shi,^{c*} Jinghua Li,^{a, b, c*}

^a The 1st Affiliated Hospital, Department of Wound Repair, Engineering Research Center of Biomaterials and Medical Devices of Hainan Province, College of Emergency and Trauma, Hainan Medical University, Haikou 570100, China

^b College of Medical Technology and Engineering, College of Materials Science and Engineering, the 1st Affiliated Hospital, Henan University of Science and Technology, Luoyang 471003, China

^c College of Chemistry and Chemical Engineering, Key Laboratory of Natural Medicine and Immune-Engineering of Henan Province, Henan University, Kaifeng 475004, China

‡These authors contributed equally to this work.

* Corresponding author: Dr. Jinghua Li

The 1st Affiliated Hospital, Engineering Research Center of Biomaterials and Medical Devices of Hainan Province, College of Emergency and Trauma

Hainan Medical University, Haikou 570100, China

E-mail: anubiss1860@163.com Tel: +86-23-65111802

List of Contents

Experiment section	S3
Fig. S1. Particle size distribution of the as-synthesized COPC-Nfs	S5
Fig. S2. Atomic arrangement of the obtained COPC-Nfs	S6
Fig. S3. XPS spectra of Cu 2p of the as-synthesized COPC-Nfs	S7
Fig. S4. UV-Vis absorbance spectrum of the as-prepared COPC-Nfs	S8
Fig. S5. Zeta potential of COPC-Nfs	S9
Fig. S6. Degradation of MB-H under different pH	S10
Fig. S7. Decoloration variance during the dye degradation process	S11
Fig. S8. TOC results for the dye degradation	S12
Fig. S9. Reusability of COPC-Nfs within 10 cycles	S13
Fig. S10. H ₂ O ₂ generation profiles	S14
Table S1. Photo degradation of dye with different nanocatalysts	S15
Table S2. Photo-electro degradation of dye with different nanocatalysts	S16
Reference	S17

Experiment section

Chemicals and Materials

All chemicals were purchased and used without further purification. Platinum acetylacetonate ($\text{Pt}(\text{acac})_2$, $\geq 99.98\%$), cetyltrimethylammonium bromide (CTAB, $\geq 98\%$), and cupric acetylacetonate, ($\text{Cu}(\text{acac})_2$) were bought from Sigma-Aldrich CO., Ltd (America). Oleylamine (OAM, 80-90%) and methylene blue (MB, 99%) were supplied by Aladdin Co., Ltd (Shanghai, China).

Fabrication of COPC-Nfs

The COPC-Nfs nanoparticles were fabricated by a solvothermally method via our previous report^[1, 2]. Typically, 39.5 mg $\text{Pt}(\text{acac})_2$, 130.0 mg $\text{Cu}(\text{acac})_2$, and 750.0 mg CTAB were dissolved in 30.0 mL oleylamine, then the mixture was added into a teflon-lined high-pressure reaction kettle (50 mL) in a 170 °C oil bath for continuous 48 h. The autoclave was then cooled down to room temperature. The black products were collected by centrifugation (3500 rpm, 5 min) and re-dispersed in cyclohexane, the obtained black nanoparticles was the oleate-capped COPC-Nfs. Then the solution was regulated to pH 4.0 by 0.1 M HCl solution. The nanoparticles are kept in 50 °C suspension for 5 h to remove the superficial oleylamine on the surface of PtCu nanoframes. The oleate-free COPC-Nfs were finally collected with a centrifuge (10000 rpm, 5 min) and washed with acetone and ethanol every 6 times.

Characterization of COPC-Nfs

The morphological feature of the obtained nanoframes was monitored by SEM (Nova-400, FEI), TEM (LIBRA 200-FEG, Zeiss) and HAADF-STEM (Titan G2

80-200, FEI). The crystalline structure of the nanoagents was measured by the XRD spectrograph (D/max 2500-PC, Rigaku). The elementary composition of the nanocomposites was recorded by an XPS Spectrometer (Quantera II, ULVAC-PHI).

Photothermal thermogenesis of COPC-Nfs

The UV-vis-NIR absorption of the nanoagents was detected by a UV-vis-NIR spectrophotometer (NanoDrop One, Thermo). Then the COPC-Nfs nanoframes with various concentrations (50, 100, 300 and 600 $\mu\text{g}\cdot\text{mL}^{-1}$) were treated by 808 nm NIR laser ($2.0\text{ W}\cdot\text{cm}^{-2}$, 5 min). A thermal infrared imager was used in this study to record the temperature variation. Next, the thermogenesis stability of the obtained COPC-Nfs was further investigated by a 6 on-off cyclic photothermal thermogenesis experiment.

Monitoring the production of Hydroxyl radicals ($\bullet\text{OH}$)

To detect the Hydroxyl radical levels induced by COPC-Nfs under DC and NIR laser treatment, we used 5, 5-dimethyl-1-pyrroline-N-oxide (DMPO) as the $\bullet\text{OH}$ specific spin-trapping agent to determine the generation of $\bullet\text{OH}$ reactive oxygen. Typically, the electrolyte is the MB-H solution (solvent: H_2O , 1.0 L), the electrode area is 19.625 mm^2 (radius: 2.5 mm). Then DMPO (0.1 mL, 0.3 M) was added to the culture plate. Finally, the DMPO-OH adduct of 1:2:2:1 characteristic peak was recorded by ESR spectrograph immediately.

Statistical analysis

All digital data were analyzed with Origin (version 7.5) via one-way variance analysis and Students' t-test. The confidence levels were set as 95% and 99%.

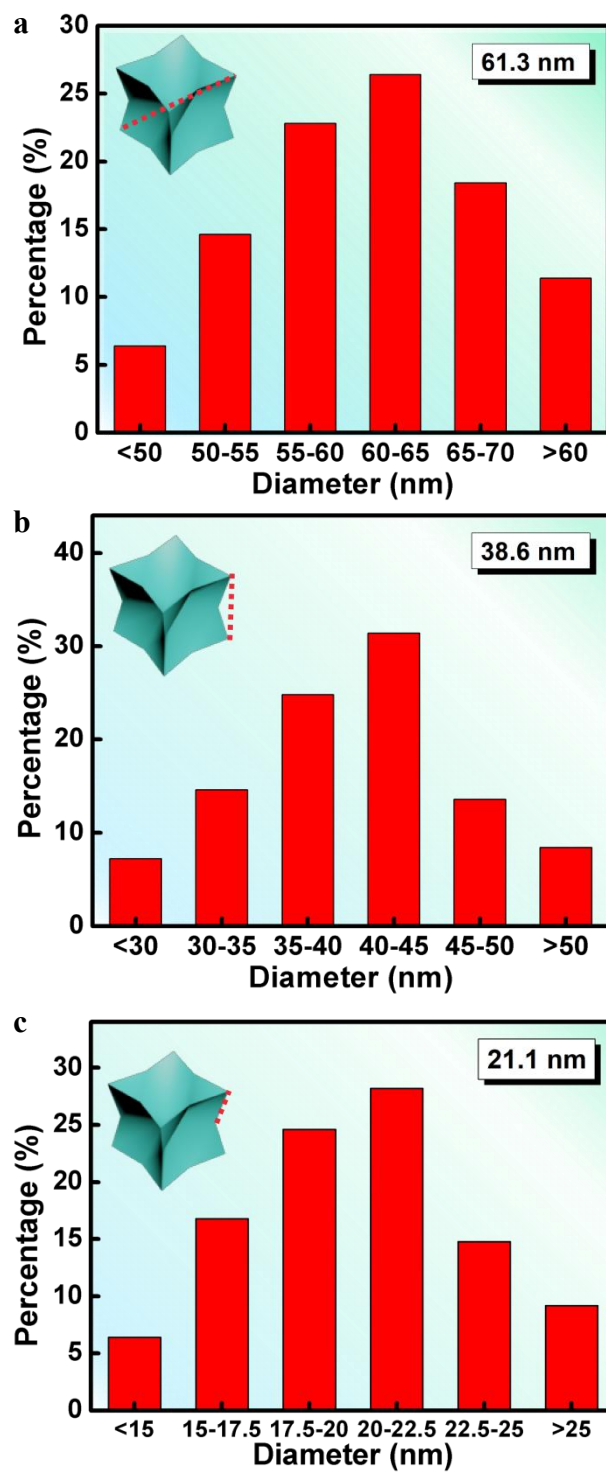


Fig. S1. Particle size distribution of the as-synthesized COPC-Nfs: **a)** diagonal length, **b)** edge breadth and **c)** feet length, respectively.

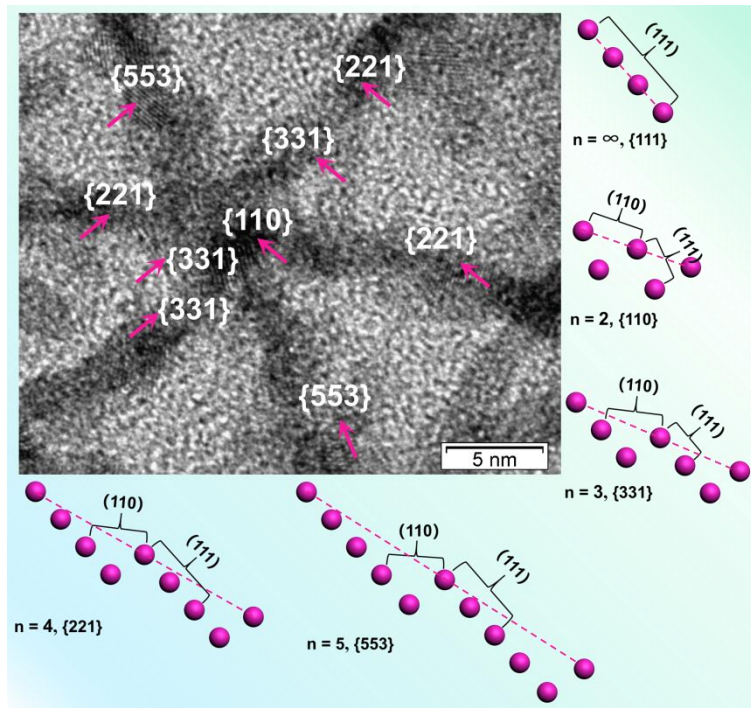


Fig. S2. Atomic arrangement of the obtained COPC-Nfs on the n -(111)-(111) surfaces.

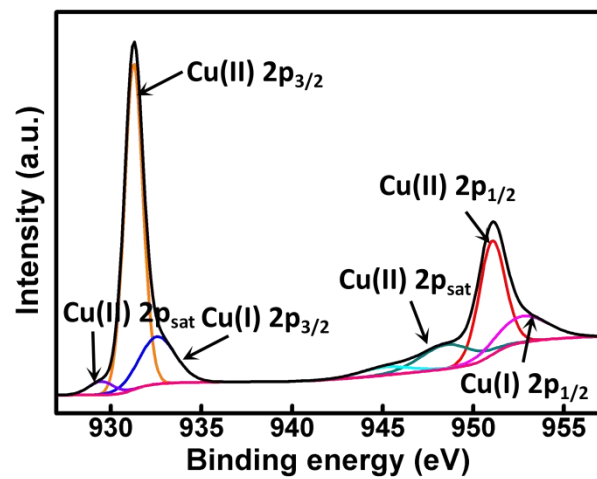


Fig. S3. XPS spectra of Cu 2p of the as-synthesized COPC-Nfs.

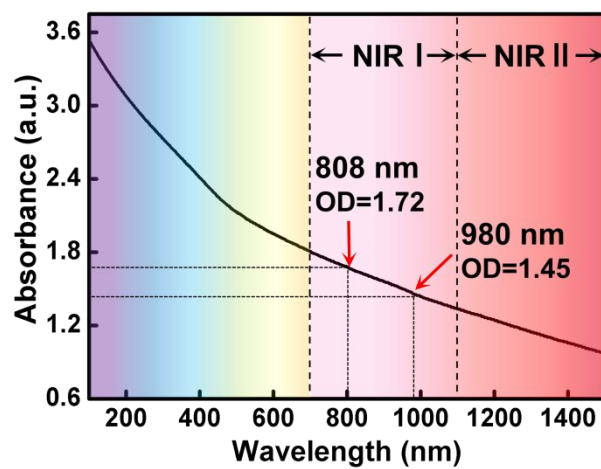


Fig. S4. UV-Vis absorbance spectrum of the as-synthesized COPC-Nfs.

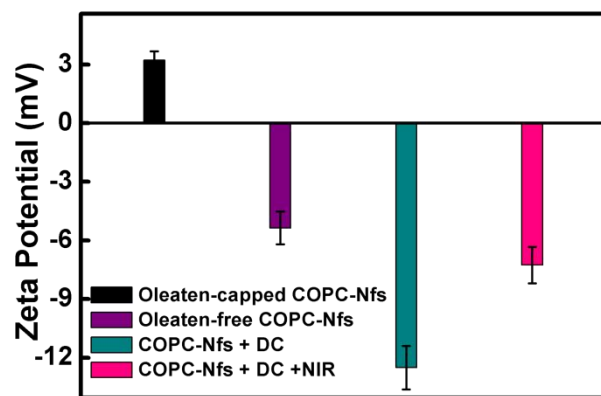


Fig. S5. Zeta potential of COPC-Nfs at various states.

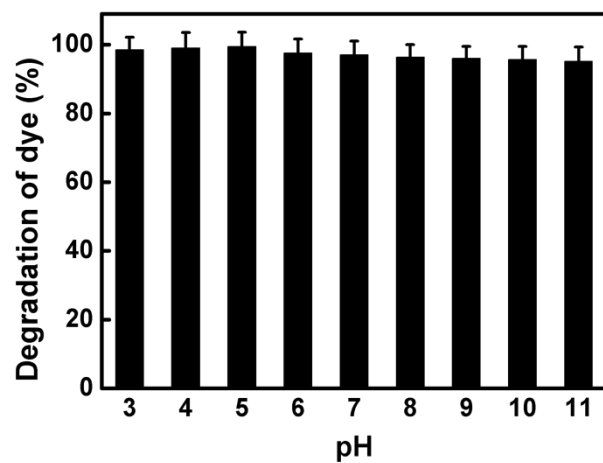


Fig. S6. Degradation of MB-H under different pH by using COPC-Nfs that treated with DC and NIR laser.

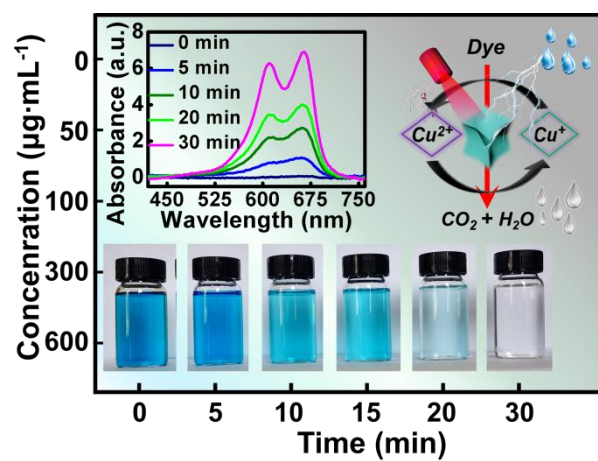


Fig. S7. Decoloration variance during the dye degradation process under NIR laser irradiation, inset: temperature-dependent Uv-Vis spectrum of dye degradation.

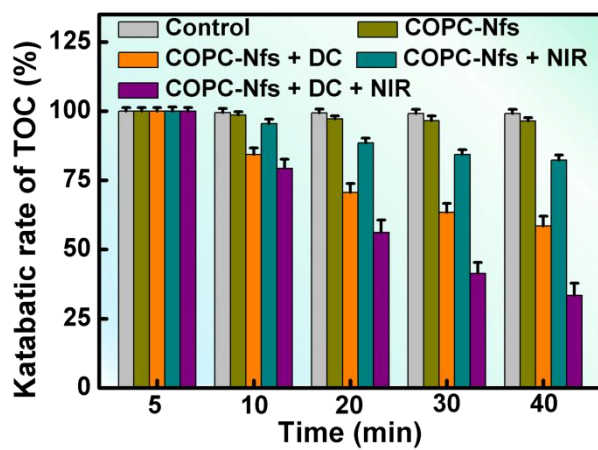


Fig. S8. TOC results for the dye degradation by using COPC-Nfs under different processed strategies.

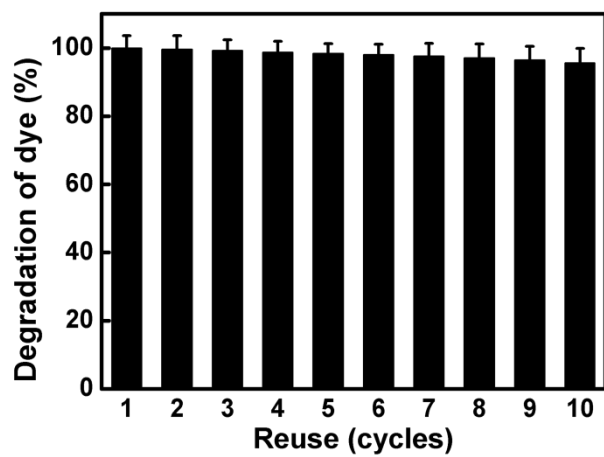


Fig. S9. Reusability of COPC-Nfs that treated with DC and NIR laser for MB-H removal within 10 cycles.

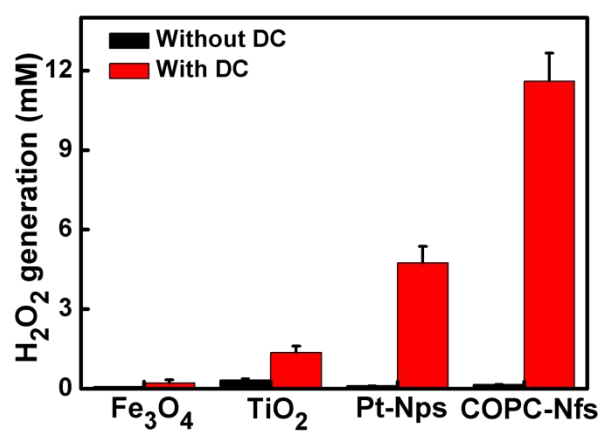


Fig. S10. H₂O₂ generation profiles triggered by different nanocatalysts under DC treatment.

Table S1. Photo degradation of Methylene Blue with different nanocatalysts.

<i>Catalyst</i>	<i>C_{dye}</i> (mg/L)	<i>Catalyst</i> (g/L)	<i>Irradiation</i> <i>time (min)</i>	<i>Wavelength</i> (nm)	<i>Degradation</i> (%)	<i>Ref.</i>
MnFe ₂ O ₄	7	0.30	120	Visible	15.1	3
MgFe ₂ O ₄	7	0.60	180	400-700 nm	26.0	4
ZnFe ₂ O ₄	10	0.60	360	400-700 nm	32.0	4
CaFe ₂ O ₄	10	1.00	360	>420 nm	28.0	5
BaFe ₁₂ O ₁₉	10	1.00	360	420-700 nm	26.0	6
COPC-Nfs	10	0.30	30	808 nm	43.9	This work

Table S2. Photo-electro degradation of dye with different nanocatalysts.

<i>Catalyst</i>	<i>Dye type</i>	<i>C_{dye}</i>	<i>DC Power</i> <i>(W)</i>	<i>Time</i> <i>(min)</i>	<i>Degradation</i> <i>(%)</i>	<i>Ref.</i>
CNP/B- BiVO ₄ /WO ₃	Orange II	50 mg/L	/	180	92.0	7
Fe (OH) ²⁺ /Fe (III)	Acid Black 172	200 mg/L	/	30	97.4	8
B-doped TiO ₂ NTs	Naphthol yellow S	50 ppm	300	120	100	9
GR/b-CD	Bromophenol blue	20 mg/L	300	180	91.5	10
TiO ₂	Methylene blue	10 mg/L	500	180	22.4	11
Co/TiO ₂	Methylene blue	10 mg/L	500	120	74.2	11
COPC-Nfs	Methylene blue	10 mg/L	500	30	99.2	This work

Reference

1. Li JH, Zhanga JB, Jiao XB, Ye JX, Song KN, Bao JF, Li GD, Lei K. NIR-driven PtCu-alloy nanocages via photothermal enhanced fenton catalytic degradation of pollutant dyes under neutral pH. *J Alloy Compd.* 2022; **895**: 162624.
2. Li JH, Zu XY, Liang GF, Zhang KK, Liu YL², Li K, Luo Z, Cai KY. Octopod PtCu nanoframe for dual-modal imaging-guided synergistic photothermal radiotherapy. *Theranostics.* 2018; **8(4)**: 1042-1058.
3. Hou X, Feng J, Xu X, Zhang M. Synthesis and characterizations of spinel MnFe₂O₄ nanorod by seed-hydrothermal route, *J Alloy Compd.* 2010; **491**: 258-263.
4. Chen CH, Liang YH, Zhang WD. ZnFe₂O₄/MWCNTs composite with enhanced photocatalytic activity under visible-light irradiation, *J Alloy Compd.* 2010; **501**: 168-172.
5. Dom R, Subasri R, Radha K, Borse PH. Synthesis of solar active nanocrystalline ferrite, MFe₂O₄ (M: Ca, Zn, Mg) photocatalyst by microwave irradiation, *Solid State Commun.* 2011; **151**: 470-473.
6. Valero-Lunaa C, Palomares-Sánchez SA, Ruíz F. Catalytic activity of the barium hexaferrite with H₂O₂/visible light irradiation for degradation of Methylene Blue. / *Cata Today*, 2016; **266**: 110-119.
7. Peleyeju GM, Umukoro EH, Babalola JO, Arotiba OA. Solar-light-responsive titanium-sheet-based carbon nanoparticles/B-BiVO₄/WO₃ photoanode for the photoelectrocatalytic degradation of orange II dye water pollutant. *ACS Omega.* 2020; **5(10)**: 4743-4750.

8. Mahmoudi N, Farhadian M, Nazar AR, Eskandari P, Esfahani KN. Investigation and optimization of the performance of sono-photo-electro-Fenton process for removal of Acid Black 172 and Disperse Blue 56 from polluted water: comparison of the degradation activity with electro-Fenton-based processes. *Int J Environ Sci Te.* 2022; **19**: 1671-1682.
9. Bessegato GG, Cardoso JC, Zanoni MV. Enhanced photoelectrocatalytic degradation of an acid dye with boron-doped TiO₂ nanotube anodes. *Cata. Today.* 2015; **240**: 100-106.
10. Cong Q, Ren M, Zhang TT, Cheng FY, Qu J. Efficient photoelectrocatalytic performance of beta-cyclodextrin/graphene composite and effect of Clin water: degradation for bromophenol blue as a case study. *RSC Adv.* 2021; **11**, 29896-29905.
11. Du YL, Zheng ZX, Chang WZ, Liu CY, Bai ZY, Zhao XY, Wang CM. Trace Amounts of Co₃O₄ Nano-Particles Modified TiO₂ Nanorod Arrays for Boosted Photoelectrocatalytic Removal of Organic Pollutants in Water. *Nanomaterials.* 2021; **11**: 214.